Dalton Transactions

PAPER

View Article Online
View Journal

CrossMark click for updates

Cite this: DOI: 10.1039/c6dt00865h

Tuning supramolecular aurophilic structures: the effect of counterion, positive charge and solvent†

Elisabet Aguiló,[a] Raquel Gavara,[a] Clara Baucells,[a] Marta Guitart,[a] João Carlos Lima,[b] Jordi Llorca[c] and Laura Rodríguez*[a]

Received 3rd March 2016,
Accepted 10th March 2016

DOI: 10.1039/c6dt00865h

www.rsc.org/dalton

The synthesis of the cationic gold(I) complexes [Au(C≡CC$_5$H$_4$N)(CH$_3$–PTA)]X (X = I, **1**; X = OTf, **4**), [Au(C≡CC$_5$H$_4$N–CH$_3$)(PTA)]X (X = I, **2**; X = OTf **5**; PTA = 1,3,5-triaza-7-phosphatricyclo[3.3.1.13.7]decane) and [Au(C≡CC$_5$H$_4$N–CH$_3$)(DAPTA)]X (X = I, **3**; X = OTf = **6**, DAPTA = 3,7-diacetyl-1,3,7-triaza-5-phosphabicyclo[3.3.1]nonane) results in cationic complexes with unexpected supramolecular assemblies in water ranging from rod-like structures (**1**) to vesicles (**2** and **3**) and square-like structures (**5** and **6**). These morphologies are completely different from the fibers previously obtained with their parent neutral complexes [Au(C≡C$_5$H$_4$N)(PTA)] and [Au(C≡C$_5$H$_4$N)(DAPTA)]. Nevertheless, the introduction of triflate as a counterion in **1** (complex **4**) gives rise to the formation of a highly soluble complex in water which does not display any significant aggregation in solution. These results reveal the importance of the introduction of a positive charge on global supramolecular assemblies and how the counterion can also modify the resulting package. Interestingly, we have also proved that the aggregation of complexes **2**, **3**, **5** and **6** is also affected by the solvent with direct influence on their absorption and emission properties and the global morphology of the aggregates.

Introduction

Topology is becoming established in material science in the study of its affects on the physical properties of materials at the nano-/mesoscale and in the study and design of materials from a topological perspective.[1] This incipient appreciation for the importance of topology in the last few years has resulted in the development of entirely new materials with unusual topologies that lead to either unusual or enhanced properties.[2–4] The self-assembly of small molecules has received great attention in this field in the past decade, not only because of their fascinating and innumerable supramolecular morphologies (including spherical or cylindrical micelles, vesicles, toroids, rods, ribbons, lamellar platelets, scrolls or nanotubes)[5] but

[a]Departament de Química Inorgànica i Orgànica, Universitat de Barcelona, Martí i Franquès 1-11, 08028 Barcelona, Spain. E-mail: laura.rodriguez@qi.ub.es; Fax: +34 934907725; Tel: +34 934039130
[b]LAQV-REQUIMTE, Departamento de Química, CQFB, Universidade Nova de Lisboa, Monte de Caparica, Portugal
[c]Institut de Tècniques Energètiques i Centre de Recerca en NanoEnginyeria, Universitat Politècnica de Catalunya, Diagonal 647, 08028 Barcelona, Spain

†Electronic supplementary information (ESI) available: Experimental section; HR-ESI(+) mass spectrum of complex **1** (Fig. S1); HR-ESI(+) mass spectrum of complex **2** (Fig. S2); HR-ESI(+) mass spectrum of complex **3** (Fig. S3); ^{1}H-NMR spectrum of **2** in D$_2$O (Fig. S4); ^{1}H-NMR spectrum of **3** in D$_2$O (Fig. S5); ^{1}H-NMR spectrum of **2** in CDCl$_3$ (Fig. S6); ^{1}H-NMR spectrum of **3** in CDCl$_3$ (Fig. S7); SEM images of dried samples of **2** (up) and **3** (bottom) (Fig. S8); *Z* potential values measured for 5×10^{-5} M solutions of **2** and **3** in water by DLS measurements (Fig. S9); ^{1}H-NMR spectrum **4** in water (Fig. S10); HR-ESI(+) mass spectrum of complex **5** (Fig. S11); HR-ESI(+) mass spectrum of complex **6** (Fig. S12); optical microscopy images of aqueous dried samples of **5** (left) and **6** (right) (Fig. S13); SEM images of aqueous dried samples of **5** (up) and **6** (bottom) (Fig. S14); absorption spectra of 5×10^{-5} M solutions of complexes **1–6** in water (Fig. S15); absorption spectra of freshly prepared *ca.* 1×10^{-4} M solution (solid line) and after 2 days (red line) of **2** in water (Fig. S16); emission spectra of **2** at three different concentrations in water. λ_{exc} = 370 nm (Fig. S17); hypsochromic effect with increasing polarity (negative solvatochromism) displayed in absorption spectra of complex **2** (Fig. S18); plot of $\bar{\nu}_{0exp}$ *vs.* $\bar{\nu}_{0calc}$ for absorption data of compound **3** (Fig. S19); plot of $\bar{\nu}_{0exp}$ *vs.* $\bar{\nu}_{0calc}$ for absorption data of compound **2** (Fig. S20); normalized emission spectra of **3** in different solvents (Fig. S21); normalized emission spectra of **4** in different solvents (λ_{exc} = 370 nm) (Fig. S22); normalized emission spectra of **5** in different solvents (λ_{exc} = 300 nm) (Fig. S23); normalized excitation spectra of **2** in different solvents (Fig. S24); optical microscopy images of **2** in water (A), methanol (B), acetonitrile (C) and CHCl$_3$ (D) (Fig. S25); optical microscopy images of **3** in water (A), methanol (B), acetonitrile (C) and CHCl$_3$ (D) (Fig. S26); optical microscopy images of **5** in water (A), methanol (B), acetonitrile (C) and CHCl$_3$ (D) (Fig. S27); optical microscopy images of **6** in water (A), methanol (B), acetonitrile (C) and CHCl$_3$ (D) (Fig. S28); synthesis of *N*-methyl-4-ethynylpyridinum iodide (Scheme S1); synthesis of *N*-methyl-4-ethynylpyridinum triflate (Scheme S2); synthesis of the *N*-methyl-4-ethynylpyridinum perchlorate derivatives (Scheme S3); absorption and emission (λ_{exc} = 370 nm) data of complexes **1–6** in water (Table S1); α, β, π^* parameters for the solvents used (Table S2); absorption data of the XLCT band of **2** and **3** in different solvents (Table S3). See DOI: 10.1039/c6dt00865h

also due to their potential applications in material science,[6] in molecular devices[9] or as mimics of biological systems or functions.[7,8]

In the last few years, gold(I) complexes have represented an emerging area of investigation within this field, as they show weak Au(I)···Au(I) aurophilic interactions[10] which can modulate and govern the resulting assemblies and properties in very different potential applications.[11] Among the resulting supramolecular structures obtained with low molecular weight gold(I) complexes, recent reports on hydrogelators should be highlighted.[12–14] The formation of these gels has been driven through non-covalent interactions, which are commonly van der Waals forces, hydrogen bonding, electrostatic attractions and π–π stacking interactions, together with aurophilic interactions.[12]

Our recent results on the formation of hydrogels from small organometallic complexes containing Au(I)–alkynyl moieties,[15–17] prompted us to go one step further in the design and synthesis of novel supramolecular nanostructures prepared by the self-assembly of small molecules. In particular, we are interested in the understanding of how supramolecular packing can be modulated by modifications of the chemical structure or the environment of small gold(I) organometallic precursors. The design and synthesis of novel self-assembling materials with tunable properties is challenging, but undeniably crucial, and the understanding of the factors that control such properties has aroused much interest in the last few years.[18–25] We are mainly interested in gold(I) alkynyl complexes, due to their appealing stems from the two-coordinate linear geometry of the metal atom and the linearity of the alkynyl moiety, which together have made them ideal candidates for the exploration of self-assembling functional properties and have drawn attention due to their wide range of different properties.[11] For these reasons, in this work, we report how the 3D assemblies of gold(I) derivatives previously reported by us[15,16] can be modulated by the introduction of different factors. In fact, we have been able to tune the large pre-organized fibrilar structures previously found and convert them into rods, spherical vesicles or square-like morphologies, among others, by the introduction of a positive charge to the chemical structure either at the phosphine unit (complexes **1** and **4** Chart 1) or at the pyridyl unit (complexes **2**, **3**, **5** and **6**). The influence of the counterion of these positively charged complexes has also been explored together with the effect of the polarity of the solvents in the intermolecular interactions giving rise to unprecedented changes in their photophysical and morphological properties. Very recently, the formation has been reported of various structures with Au alkynyl amphiphilic systems and different long alkyl chains.[18] But the absence of these long alkyl chains in our complexes make them particularly appealing with regard to the study of their aggregation processes. And, to the best of our knowledge, this is the first example, with this family of compounds, that shows how the polarity of different solvents and the presence of different counterions can induce the formation of distinct supramolecular structures in solution. On the other hand, as was observed for the effect of solvent vapours on the resulting luminescent properties of organometallic gold(I) complex crystals,[26–30] the rearrangements that occur in solution, also affect the emission of the aggregates.

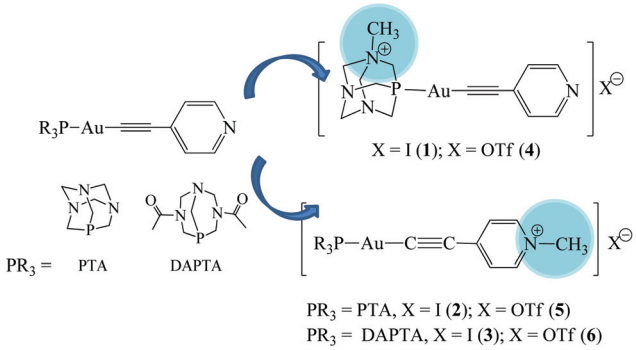

Chart 1 Positively charged species studied in this work.

Results and discussion

Synthesis and characterization

Complex **1** was obtained by the reaction of [Au(C≡CC$_5$H$_4$N)(PTA)] with CH$_3$I at low temperature (Scheme 1). Previously, we carried out the reaction involving [Au(C≡CC$_5$H$_4$N)]$_n$ and (PTA-Me)I but this was not accomplished successfully. On the other hand, positively charged complexes of the pyridyl unit were also obtained by modifications of the synthetic procedures (Scheme 2). For this, the previous synthesis of the organic ligand *N*-methyl-4-ethynylpyridinum iodide was necessary (Scheme S1†). In these cases, the acac method[31] was necessary to remove the terminal alkynyl proton, and complexes **2** and **3** were obtained with moderate yields (*ca.* 50–70%).

Characterization of complexes **1–3** by ^{1}H, ^{31}P-NMR and IR spectroscopy, and mass spectrometry verified the successful formation of these products. In all the cases, molecular peaks were displayed in the ESI-MS experiments (Fig. S1–S3†). The corresponding C≡C and C=N vibrations of the chromophoric units were also observed in the IR spectra in all the cases. Most importantly, the disappearance of the terminal alkynyl proton detected by IR and ^{1}H-NMR is clear evidence of the formation of complexes **2** and **3**. Additionally, the characteristic H$_\alpha$ and H$_\beta$ protons of the pyridine together with the characteristic patterns of PTA (**2**) or DAPTA (**3**) phosphines in D$_2$O were observed in the ^{1}H-NMR spectra of the complexes (Fig. S4 and S5†). The formation of aggregated samples in this solvent was evidenced by the presence of different H$_\alpha$ and H$_\beta$ pyridyl protons where this moiety must be directly affected.[15,16] Only phosphine protons were detected in chloroform, due to the poor solubility of the ionic part of the molecules in apolar solvents (Fig. S6 and S7†).[15–17,32–34] Moreover, the more asymmetric pattern of the methylated phosphine (**1**) was also recorded by ^{1}H-NMR in D$_2$O (Fig. 1 top).[35–37] Interesting findings were observed from ^{1}H-NMR characterization in D$_2$O. The corresponding spectra of the three complexes clearly displayed

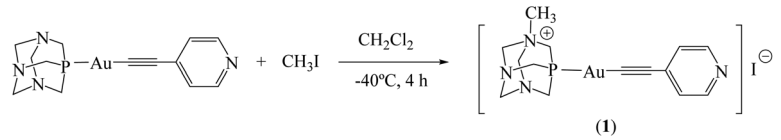

(1)

Scheme 1 Synthesis of [Au(C≡C$_5$H$_4$N)(PTA-Me)]I complex.

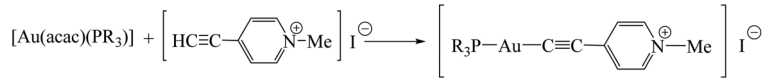

PR_3 = PTA (**2**); DAPTA (**3**)

Scheme 2 Synthesis of [Au(C≡C$_5$H$_4$N-Me)(PR$_3$)]I (PR$_3$ = PTA, DAPTA) complexes.

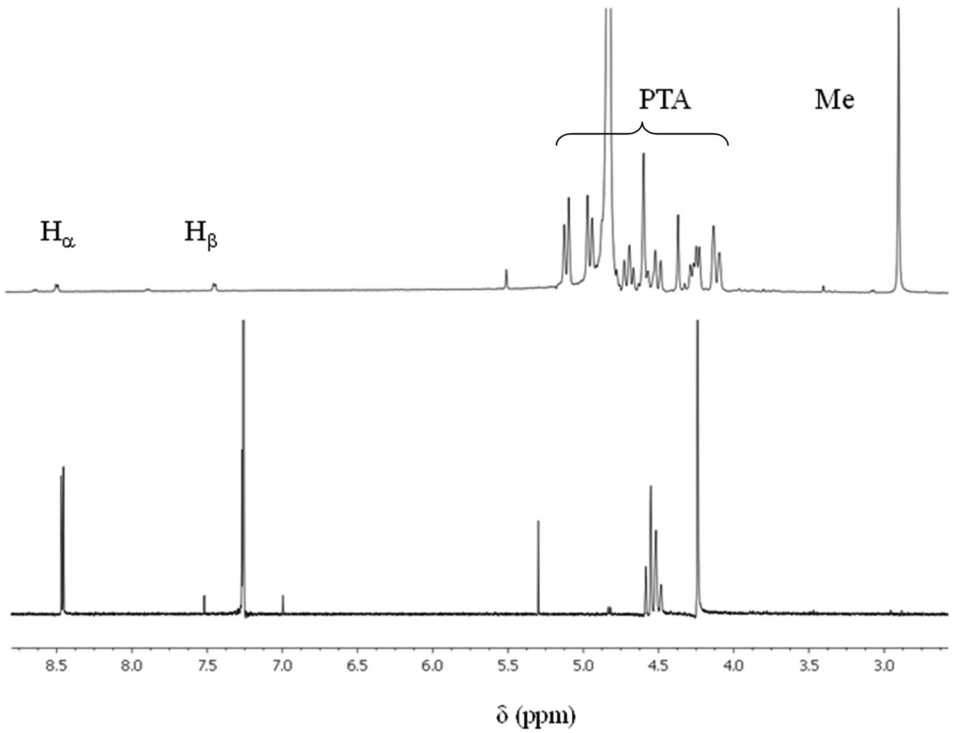

Fig. 1 ^{1}H-NMR spectrum of complex **1** in D_2O (top) and in $CDCl_3$ (bottom). H_β protons in the spectrum below are buried under the $CDCl_3$ signal.

the characteristic protons of the phosphines while protons of the ethynylpyridyl chromophore could only be observed (and with very low intensity) in diluted conditions (Fig. 1 top). Similar behaviour was recently observed for the [Au(C≡C$_5$H$_4$N)(PTA)][15] complex which is proof that aggregation occurs in this solvent, and the organic chromophoric unit must be directly involved. In the absence of aggregation, (as observed in $CDCl_3$, Fig. 1 bottom) the ^{1}H-NMR spectrum shows the correct integration ratio of 2 : 6 between the pyridyl H_a and phosphine protons. For the reasons detailed above, some kinds of supramolecular assemblies were also expected for **1–3** in water. Nevertheless, the lack of the expected gel behaviour of the solutions did not indicate the formation of long fibers promoting gelification in these cases (see below).

In **1**, the phosphine groups are expected to point towards water molecules while the more hydrophobic ethynylpyridyl moieties are expected to pack closely to each other through hydrophobic interactions. In the case of **2** and **3**, the presence of a positive charge at the pyridyl groups is expected to promote a different aggregation pattern, where the positively charged unit is located towards the water molecules. This hypothesis was also confirmed by the *Z* potential values measured by Dynamic Light Scattering (DLS) experiments (see below).

Analysis of the aggregates by electron microscopy and optical microscopy

Scanning electron microscopy was used as an important tool for gaining insight into the supramolecular assemblies of

these complexes and to analyse the effect of the positive moiety (**1–3**) in the resulting, and unpredictable, three-dimensional supramolecular packing. The rod aggregates of **1** were about 20–30 μm long; the individual spherical aggregates of **2** and **3** measured around 20 nm and the presence of a multilayer system (typical of vesicles), containing in some cases hollows (darker colour) with an empty inner, was detected for **2** (Fig. 2). Moreover, the spherical aggregates seemed to agglomerate to sizes of *ca*. 200 nm or greater (Fig. S8†). Cryogenic transmission electron microscopy (cryo-TEM) images provided key evidence for verification of the presence of the micellar-vesicles topologies of **2** and **3** in solution (Fig. 2D).

Interestingly, these morphologies seem to be maintained in larger structures and are detectable by optical microscopy (Fig. 3).

Hence, it seems clear that cationic charges produce a clear effect on the global morphology of the supramolecular assemblies and preclude the formation of long empty fibers previously observed for their neutral analogous complexes [Au(C≡C_5H_4N)(PTA)][15] and [Au(C≡C_5H_4N)(DAPTA)].[16]

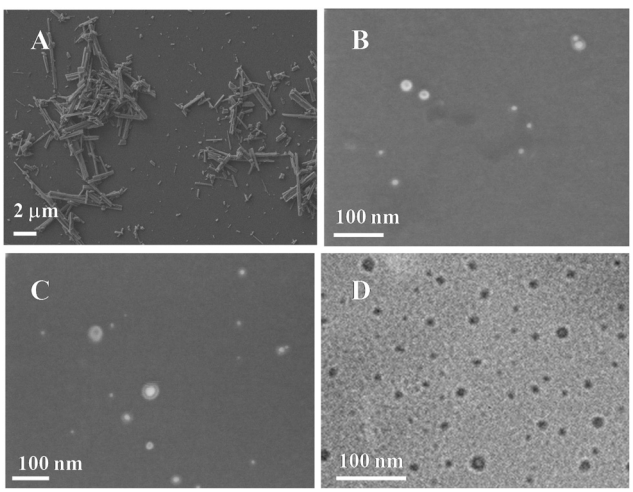

Fig. 2 Scanning electron microscopy images of dried samples of **1** (A), **2** (B) and **3** (C). Cryogenic transmission electron microscopy image of sample of a 5×10^{-4} M aqueous solution of **2** (D).

Dynamic light scattering

DLS experiments were carried out on the spherical samples (vesicles) using 5×10^{-5} M solutions and indicated that the expected size of the vesicles was around 20 nm with a positive *Z* potential value of around +25 and +15 mV for **2** and **3**, respectively (Fig. S9†). These data suggest that the positive charge may be pointing outwards in the vesicles' structure. The lowest positive value measured for **3** could be attributed to the larger steric hindrance of the DAPTA phosphine which must be related to the different packing structure (see below). DLS experiments carried out at different concentrations showed that the smaller vesicles' size are detected at *ca*. 10^{-5} M (~20 nm), and they agglomerate up to *ca*. 130–140 nm at *ca*. 1×10^{-4} M concentration (Fig. 4), in agreement with data retrieved from SEM experiments (see above). Thus, we suspect that the spherical shape is maintained both in solution and in dried samples.

To the best of our knowledge, this type of vesicles topology is the first example of weak interactions with low molecular weight complexes reported in the literature. Only small micelles have very recently been found with a Au(I)-metallo-amphiphile in buffered water.[38]

Effect of counteranion on the resulting package. The nature of the counterion can affect the resulting supramolecular package as observed in other gold supramolecular structures.[39] With this in mind, the complex [Au(C≡C_5H_4N)(PTA-Me)]OTf (**4**) was synthesized following a procedure similar to the one used to obtain **1** but using MeOTf instead of MeI. The resulting product was observed to be highly soluble in polar solvents and is shown in the corresponding ^{1}H-NMR spectrum in D_2O, which shows all the protons of the molecule in the correct integrating ratio (Fig. S10†). Thus, no significant aggregation was expected and consequently, complex **4** does not seem to give rise to the formation of highly preorganized and ordered structures.

The synthesis of *N*-methyl-4-pydidylethynyl triflate ligand was also performed following a similar procedure that for the synthesis of the iodide ligand (Scheme S2†) in order to investigate whether the counteranion could induce changes in the spherical-type aggregates observed for **2** and **3**. The introduction of other counteranions such as perchlorate was also attempted (see Scheme S3†) but the very low yield (~2%) of the

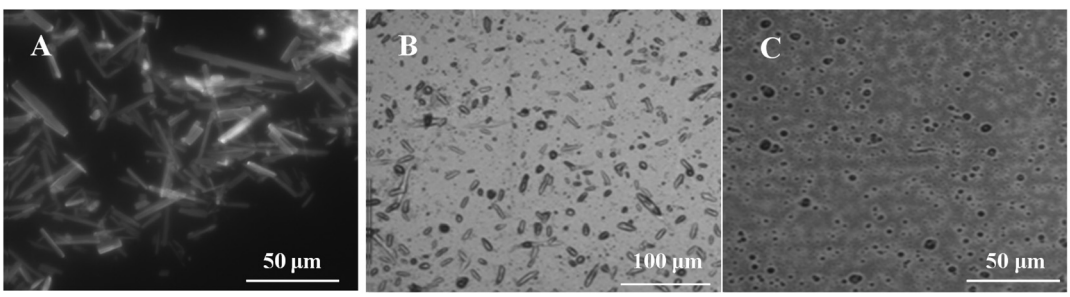

Fig. 3 Optical microscopy images of dried samples of **1** (A), **2** (B) and **3** (C).

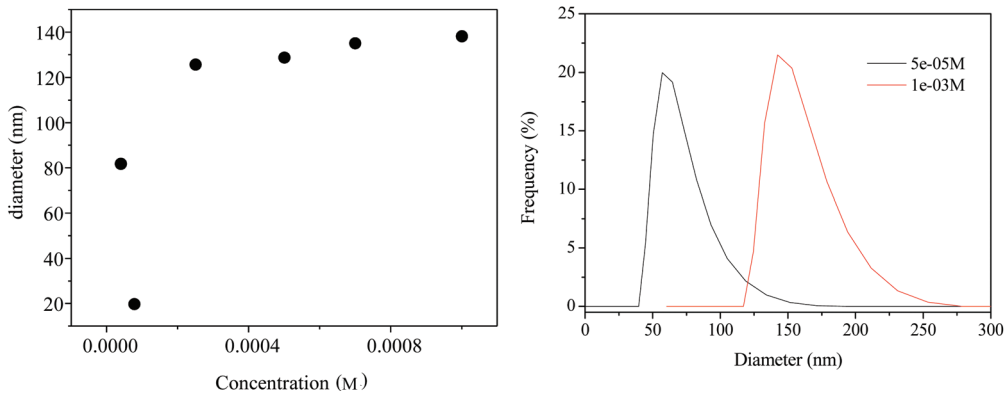

Fig. 4 Diameter of vesicles in different solutions of **2** in water at different concentrations measured by DLS (left); DLS distribution at two different concentrations: 5×10^{-5} M, black line, and 1×10^{-3} M, red line (right).

resulting organic precursor and the oily nature of the obtained gold(I) derivatives precluded their correct isolation and corresponding studies.

The reaction of the triflate ligand with [Au(acac)(PR_3)] (PR_3 = PTA, DAPTA) was accomplished by the same procedure shown in Scheme 2 for iodide derivatives and the resulting [Au(C≡C_5H_4N-Me)(PR_3)]OTf (PR_3 = PTA (**5**), DAPTA (**6**)) were successfully obtained in moderate-high yields (*ca.* 70–80%) in agreement with characterization data (Fig. S11 and S12†). Optical microscopy images of dried aqueous samples of **5** and **6** showed the formation of large structures presenting *square-like* concentric shapes (Fig. 5A and S13†). SEM characterization confirms this fact and enabled us to measure their size as *ca.* 20–40 μm (Fig. 5B and C and S14†). It could be seen that the use of a different counteranion (triflate instead of iodide) modulates the formation of different supramolecular packages: squares for triflate complexes instead of micelles/vesicles, observed for iodide derivatives (Table 1).

Analysis of the packing parameter and relation to the observed geometry. The critical packing parameter (CPP) is known to be an important tool for the determination of the geometry of micellar types of aggregates. CPP is based on the calculation of the ratio $v/(l_{max} \times a)$ where v is the volume of one molecule, l_{max} is the length of the hydrophobic part and a is the area of a cross section of the more hydrophilic part of the molecule involved in the aggregate. Calculation of the CPP values corresponding to the cationic part of the molecules (involved directly in the packing formation) was carried out by measuring the length of each molecule based on simple Spartan models (Fig. 6). The calculated CPP values were 0.51, 1.01 and 4.07 for [Au(C≡C-C_5H_4N)(CH_3PTA)]$^+$, [Au(C≡C-C_5H_4N-CH_3)(PTA)]$^+$ and [Au(C≡C-C_5H_4N-CH_3)(DAPTA)]$^+$, respectively. This is in agreement with the formation of hexagonal preferred aggregate structures for the complex with the cationic charge located at the phosphine (Fig. 6 left) and lamellar aggregates (Fig. 6 middle) and reversed micelles (Fig. 6 right) for the aggregation of complexes with the positive charge at the pyridyl moiety and PTA and DAPTA phosphines, respectively.[40] Lamellar structures tend to minimize the interactions between water molecules and the hydrophobic parts that are inside the lamellar phase. At the same time, the positively charged head groups induce a curvature, closing the structure, which also minimizes the repulsion between the positively charged head groups and results in the formation of a vesicle.[41] This is in agreement with the characterization images obtained by SEM (see above). Finally, the high steric hindrance of the DAPTA phosphine must be responsible for the formation of reversed micelles, instead of vesicles, where the most bulky group (phosphine) is located outside the cavity. The presence of amines in this

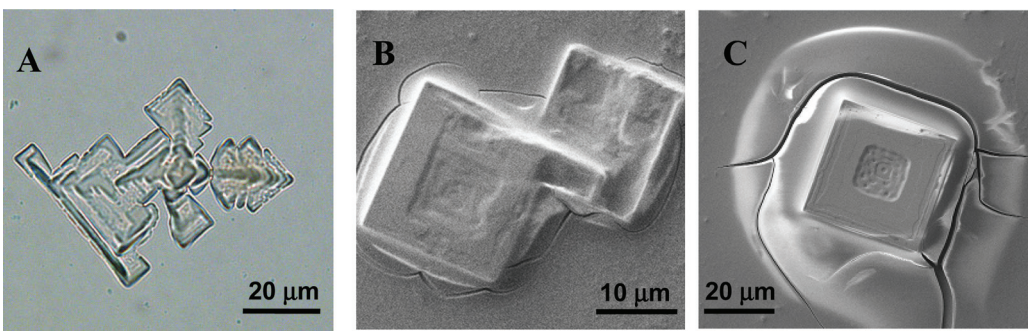

Fig. 5 Optical microscopy images of aqueous dried samples of **6** (A). SEM images of aqueous dried samples of **5** (B) and **6** (C).

Table 1 Summary of the different supramolecular assemblies of complexes **1–6** in water

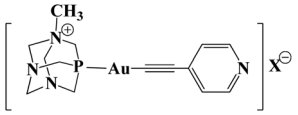	X = I^- (**1**) X = OTf^- (**4**)	Rods No significant aggregation
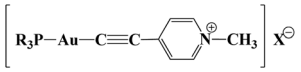	PR_3 = PTA; X = I^- (**2**) PR_3 = PTA; X = OTf^- (**5**) PR_3 = DAPTA; X = I^- (**3**) PR_3 = DAPTA; X = OTf^- (**6**)	Vesicles Square-like Vesicles Square-like

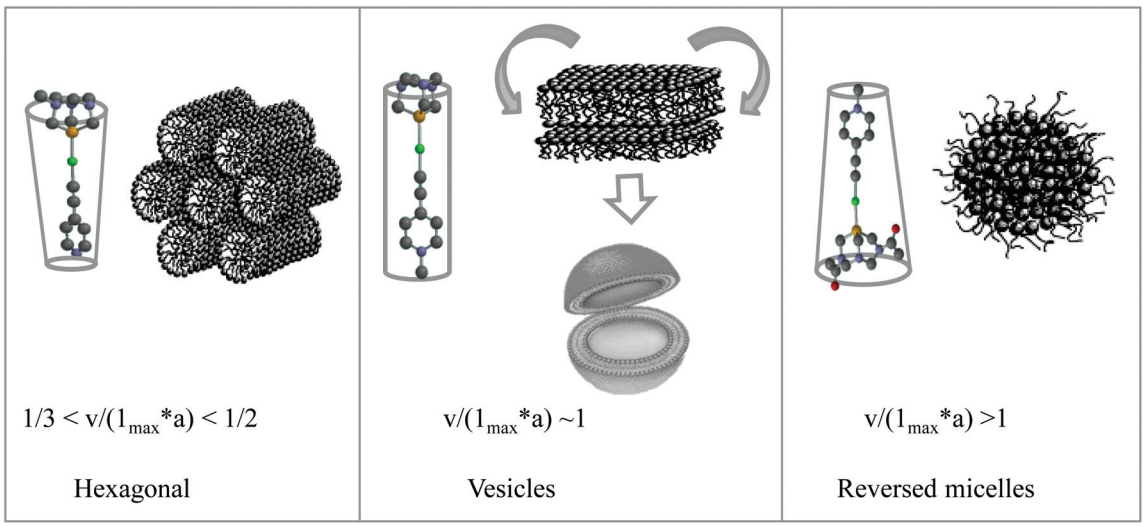

Fig. 6 Critical packing parameters (CPPs) and preferred aggregate structures for geometrical packing of $[Au(C{\equiv}C\text{-}C_5H_4N)(CH_3PTA)]^+$ (left), $[Au(C{\equiv}C\text{-}C_5H_4N\text{-}CH_3)(PTA)]^+$ (middle) and $[Au(C{\equiv}C\text{-}C_5H_4N\text{-}CH_3)(DAPTA)]^+$ (right).

phosphine makes this location possible since amine may be protonated at neutral aqueous pH.

It is known that simple inorganic counterions are very loosely associated with micelles. They are very mobile and there is no specific complex formed with a defined distance from the external part of the micelle. Thus, iodide counterions of **1–3** are not expected to affect the resulting packages and CPP could give a reasonable explanation for the packing.

We are not convinced that the same is true for triflate derivatives **4–6**, due to their lower water solubility and the evidence for a possible anion–π interaction with compound **4** (see below). The very different structures of the aggregates of **5** and **6** suggests that the packing must take into account the possible intercalation of triflate in the aggregates, nevertheless, we cannot prove this. In such a case (triflate intercalation in the structure), repulsions between the positive moieties may be less important and for this, the resulting packages are extended structures of lamellar phase giving rise to square-like samples instead of vesicles.

In order to gain more information about the packing of our structures, several attempts were made to grow single crystals suitable for X-ray diffraction but they were unsuccessful. In any case, it seems credible that the observed assemblies studied in this work are globally the result of aggregation in solution and it is not mandatory to maintain the possible packing in the solid state in the aggregates obtained in solution. They are more similar to micellar type structures than to crystalline type structures in terms of the hydrophobic/hydrophilic balance, interactions with solvent and electrostatic repulsions that determine the shapes of the aggregates.

Effect of the solvent on the resulting package. Diluted solutions of complexes **2** and **3** present different colours in polar and apolar solvents. Hence, the effect of the polarity of the solvent on the resulting spectroscopic properties and morphology was investigated.

Absorption and emission characterization in water

Absorption and emission spectra of complexes **1–6** were recorded in water at *ca.* 10^{-5} M concentration and the results are summarized in Table S1,† Fig. 7, S15† and Fig. 8. The absorption spectrum of **1** presents an intense absorption at *ca.* 265–300 assigned to intraligand (IL) π–π* (C≡Cpy) transitions based on the literature.[11,15,16,42,43] This transition exhibits some broadening (not completely vibronically resolved) which is indicative of an aggregation process where the Au–C≡Cpy moiety is directly involved.[15] Thus, π–π stacking together with aurophilic interactions are expected to be present in solution and should be responsible for the formation of the rod-like

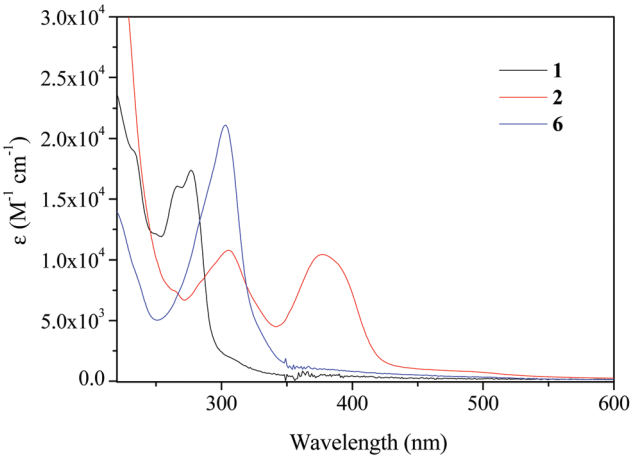

Fig. 7 Absorption spectra of 5 × 10^{-5} M solutions of complexes **1**, **2** and **6** in water.

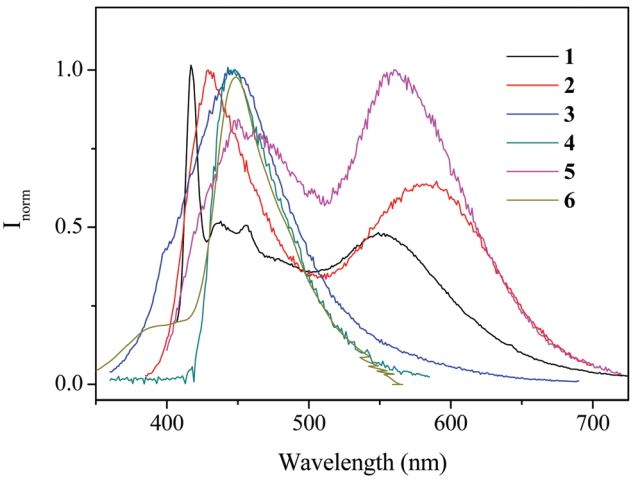

Fig. 8 Emission spectra of 2.5 × 10^{-5} M solutions of complexes **1–6** in water (λ_{exc} = 370 nm).

structures. A lower intensity broad band or tail above 300 nm can be assigned to a $\sigma^*_{Au\cdots Au}$–π^* transition according to theoretical studies carried out recently for analogous neutral complexes.[42,44] The intra-ligand absorption band of **2–6** is about 20 nm red-shifted and without vibronical resolution. In the case of **2**, **3**, **5** and **6**, this is due to the methylated pyridyl group.

Another band around 400 nm was recorded for the PTA complexes **2** and **5**. This band is probably due to the absorption of aggregated species since PTA complexes aggregate more easily than their DAPTA analogues. An additional transition around 450 nm was recorded for fresh solutions of **2** and **3** and has been tentatively assigned to XLCT transitions (X = halide), as reported in the literature for other organometallic compounds.[45,46] This charge transfer transition is favoured by the coordination of an electron withdrawing group (Au–phosphine) to the pyridinium moiety[47] and was observed to disappear in aged solutions (Fig. S16†). This is probably due to reorganization of the iodide anions in the aggregates with time.

A different profile was displayed for **4** (Fig. S16†). The highest recorded extinction coefficient is in agreement with the lack of formation of aggregates. Nevertheless, the profile is not completely understood since it resembles the spectra of the methylated pyridyl derivatives (**2**, **3**, **5** and **6**) but the ^{1}H-NMR spectra does not show any upfield shift typical for this coordination. The largest ^{1}H-NMR downfield shift of H_α and H_β protons of **4** together with the smaller calculated coupling constants, are in agreement with a possible anion–π stacking disposition.[48] Thus, the triflate counterion could interact with the aromatic pyridyl ring giving a red-shifted and unresolved absorption band. These interactions may be favoured for this counterion possibility because of hydrogen bonding and could be the reason for the different package observed by SEM.

Emission spectra, recorded upon excitation of all the samples at 370 nm, displayed the presence of a broad band around 450 nm (or vibronically structured with progressive spacings at *ca.* 2000 cm^{-1}, in the case of **1**) and an additional band near 600 nm for the PTA derivatives **1**, **2** and **5** (Fig. 8). The vibronical resolved observed in **1** let us assign this higher energy band to an intra-ligand ^{3}[π–π*(alkynyl)] emission origin. This resolution was lost for the methylated pyridyl derivatives **2**, **3**, **5** and **6**, as was observed for other methyl–pyridinium compounds.[45,46,49] The lower energy emissions may be attributed to MMLCT transitions within the aggregates as recently observed for platinum alkynyl derivatives and for the emission spectra recorded at different concentrations (Fig. S17†).[50,51] The recorded yellow emission was also in agreement with this assignment and with the fact that approximation of Au centers increases the emission in this region of the spectrum.[42] An XLCT origin should be ruled out since it is also observed for triflate derivatives and also for aged solutions where the XLCT absorption band disappears.

Absorption and emission in solvents of different polarity

It was observed that complexes **2** and **3** displayed different colours when dissolved in water and in chloroform. In order to check the effect of the solvents in the corresponding solutions, 1 × 10^{-3} M samples of complexes **2**, **3** and their triflate analogous **5** and **6** in solvents of different polarity were prepared and their absorption and emission spectra were recorded. No solvent effect was observed by the naked eye for **1** and **4**. As displayed in Fig. 9, the solutions of **3** present a wide range of different colours, and for this, their solvatochromic behaviour and the corresponding spectroscopic properties and the resulting package were investigated.

Absorption and emission spectra were measured for freshly prepared samples in the different solvents and the multiparametric method of Kamlet and Taft,[52] in which UV-Vis absorption and emission energies are correlated with different solvent properties according to eqn (1), was applied.[53–57] In this equation, $\bar{\nu}_0$ is the value of the absorption and/or emission energies in a reference solvent (cyclohexane; $\alpha = \beta = \pi^* = 0$), α is an index of the solvent's ability to act as a hydrogen-bond

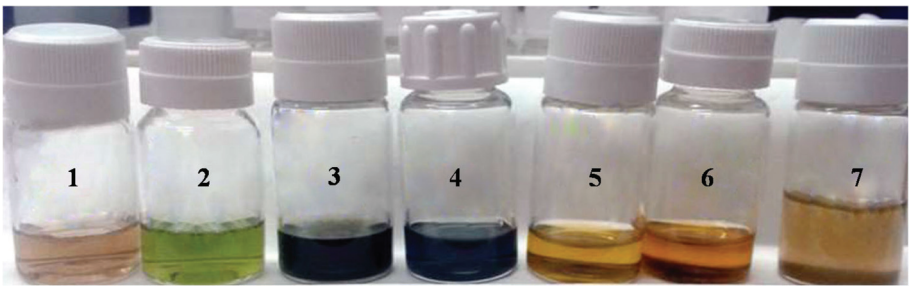

Fig. 9 1×10^{-3} M solutions of **3** in solvents of different polarity (1, water; 2, methanol; 3, acetonitrile; 4, chloroform; 5, THF; 6, toluene; 7, cyclohexane).

donor (or electron pair acceptor) toward a solute and β is a measure of the ability of a bulk solvent to act as a hydrogen-bond acceptor (or electron-pair donor), π^* is an index of the solvent polarity/polarizability which measures the solvent's ability to stabilize a neighbouring charge or dipole through non-specific dielectric interactions and δ is the polarizability correction for different classes of solvent (aliphatic, aromatic or halogenated). Often, the contribution of δ is negligible leading to the simplified eqn (2), from which the parameters a, b and p (corresponding to the responses of the appropriate solute molecular property to the relevant solvent property) can be retrieved through a multiparametric fitting for various solvents. α, β and π^* are tabulated values (Table S2†).

$$\bar{\nu} = \bar{\nu}_0 + a\alpha + b\beta + p(\pi^* + d\delta) \quad (1)$$

$$\bar{\nu} = \bar{\nu}_0 + a\alpha + b\beta + p\pi^* \quad (2)$$

The absorption band around 450 nm of compounds **2** and **3** in water was observed to be strongly dependent upon solvent polarity (Table S3† and Fig. 10 and S18†). Interestingly, this band does not appear for triflate derivatives (**5** and **6**) which is in agreement with the previous XLCT assignment (X = I^-), and the solvatochromic effect was not detected. A large negative solvatochromism (hypsochromic effect) was observed for **2** and **3** (62 nm and 65 nm respectively (~155 000 cm^{-1})) due to stabilization of the ground state in more polar solvents during the transition. Kamlet–Taft multiparametric fitting (Table 2 and Fig. S19 and S20†) shows that the polarity/polarizability (measured by π^* parameter) is the main effect on this hypsochromic shift (larger p value), which means that the stabilization by H-bonding of the ground state is less important and even less for the DAPTA derivative, **3**. Nevertheless, the ability to establish or to accept H-bonds between solvent and solute is not negligible. In fact, both a and b values are positive, and indicate a stabilization of the ground state, increasing the energy of the transition.

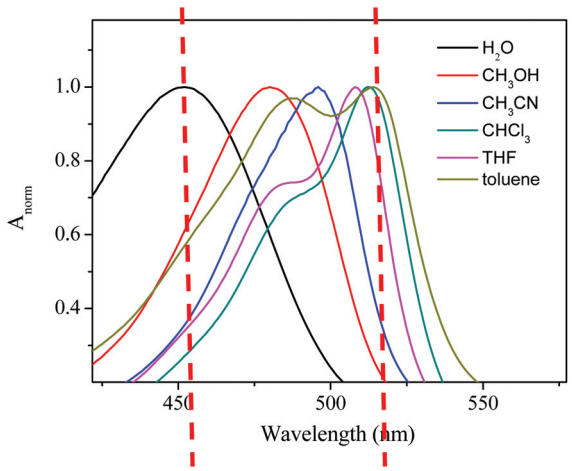

Fig. 10 Normalized absorption spectra of complex **3** recorded in different solvents. Hypsochromic effect with increasing polarity (negative solvatochromism) is shown.

Interesting findings may be retrieved from emission spectra recorded for all different solvents upon excitation at the lowest energy absorption band (*ca.* 370 nm). Two different emission bands at *ca.* 450 nm and 550 nm were recorded for all of the complexes as exemplified for **2** in Fig. 11 (see also Fig. S21–S23† for the other complexes). In the case of **2** and **5**, the general observed trend is that the lowest energy emission band increases in intensity with the solvent polarity. In the less polar solvents, such as chloroform, THF, toluene and cyclohexane, the band at 550–600 nm drastically disappears. By comparison with previous studies[15,16] the broad emission shape of both bands seems to be assigned to emissive aggregates. The lowest energy emission band recorded in polar solvents may indicate the formation of larger structures in these media in agreement with NMR data. A particular case is the emission spectrum recorded in cyclohexane (less polar solvent) which displays a different profile with a vibronically structured shape (see Fig. 11). This could be attributed to the emission of a monomer, which is in agreement with previous works.[15,16]

Table 2 a, b, p and $\bar{\nu}_0$ values, in cm^{-1}, as well as slope and correlation coefficients obtained from Kamlet–Taft multiparametric fitting of the absorption data

Compound	a	b	p	$\bar{\nu}_0$	Slope	r^2
2	942	959	2537	17 789	1	0.99
3	726	707	3288	17 430	1	0.99

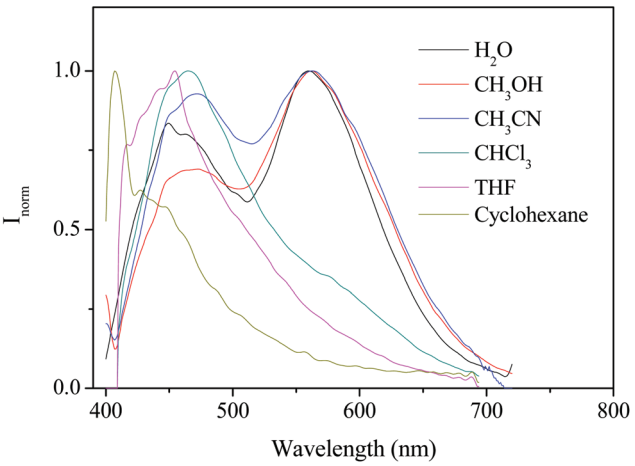

Fig. 11 Normalized emission spectra of 5 × 10^{-5} M solutions of **2** in different solvents (λ_{exc} = 370 nm).

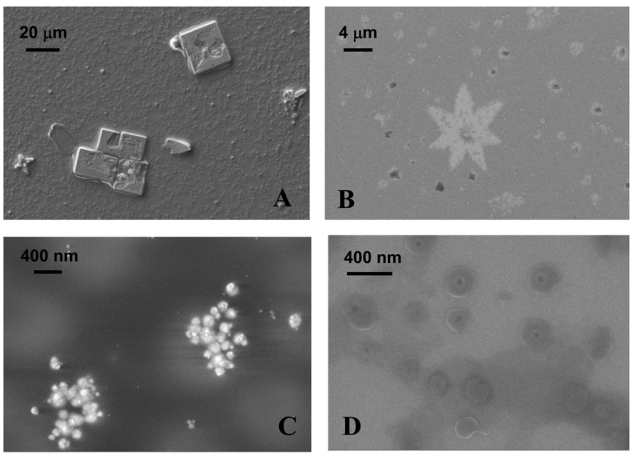

Fig. 12 SEM images of dried samples of **5** in water (A), methanol (B), acetonitrile (C) and $CHCl_3$ (D).

Excitation spectra collected at the emission maxima display two different bands centred at *ca.* 350 nm (more apolar solvents) and an additional band 450 nm (only observed in more polar solvents) corresponding to absorption of the less and more aggregated samples (see Fig. S24†).

No emission bands were displayed for **3** and **6** in less polar solvents upon excitation of the samples at 370 nm (absorption of larger aggregates). Excitation of these samples at the lower absorption wavelength (*ca.* 300 nm) gives rise to emission bands centred at *ca.* 350 nm and 450 nm. This fact is in agreement with the higher solubility of the DAPTA complexes with respect to the analogous PTA derivatives.

Analysis of the samples with different solvents using microscopic techniques

The dried samples were also observed under optical microscopy and SEM in order to correlate the morphology of the aggregates with the observed absorption and emission bands. No supramolecular structures could be detected for the samples prepared in cyclohexane, which together with the lack of the broad emission at 550–600 nm, corroborates the fact that emissive aggregates are responsible for this emission. On the other hand, different topologies were detected in the remaining solvents, which means that in all cases supramolecular structures were obtained and that these different shapes can be correlated with the different spectroscopic emission patterns recorded (Fig. 12 and S25–28†).

It is accepted in the literature that the presence of aurophilic interactions can produce long wavelength luminescent crystals that are responsive to changes in their environment.[58–60] In particular, many gold crystalline complexes display solvo- or vapoluminescence that is a result of uptake of solvent molecules into the solid phase. Nevertheless, to the best of our knowledge, this is the first report where it is shown how solvents promote the formation of different supramolecular shapes of gold(I) alkynyl aurophilic aggregates.

Conclusions

We have demonstrated how to modulate the resulting supramolecular morphology of gold(I) alkynyl complexes by carrying out different modifications of their chemical structure and environment. The effect of the introduction of a positive charge let us create rod-like structures with cationic charge located at the PTA phosphine (complex **1**). This morphology completely changes to the formation of vesicles or reversed micelles when this charge is located on the pyridyl unit (complexes **2** and **3**).

Changing the counterion from iodide to triflate gives rise to a different supramolecular package and results in the formation of square-like assemblies (complexes **5** and **6**) in water, while the higher solubility of the triflate analogues of **1** (complex **4**) precludes the formation of aggregates. Hence, we can modulate the formation of different types of 3D structures formed by the establishment of weak interactions between molecules (mainly aurophilic interactions).

The solutions of complexes **2**, **3**, **5** and **6** in different solvents enables us to demonstrate that this parameter also affects the resulting supramolecular package as could be seen by the corresponding emission spectra and microscopy images. Moreover, Kamlet–Taft multiparametric analysis of the XLCT absorption band of complexes **2** and **3** indicates that the observed negative solvatochromism in absorption is mainly due to polarity/polarizability effects while solvent polarity affects the resulting emission of the aggregates.

Experimental section

General procedures

All experiments were carried out under prepurified N_2 using standard Schlenk techniques. All of the solvents were distilled from appropriated drying agents. Commercial reagents 1,3,5-triaza-7-phosphatricyclo[3.3.1.13.7]decane (PTA, Aldrich

97%), 3,7-diacetyl-1,3,7-triaza-5-phosphabicyclo[3.3.1]nonane (DAPTA, Aldrich 97%), MeI (Aldrich, 99%) and $MeCF_3SO_3$ (Aldrich, 99%) were used as received. Literature methods were used to prepare *N*-methyl-4-ethynylpyridine iodide,[60] [AuCl(PTA)],[61] [AuCl(DAPTA)],[61] [Tl(acac)][62] and [Au(C≡C-C_5H_4N)(PTA)].[15] A similar procedure to that previously reported for *N*-methyl-4-ethynylpyridine iodide was used for the synthesis of *N*-methyl-4-ethynylpyridine triflate,[63] but $MeCF_3SO_3$ was used instead of MeI.

Physical measurements

Infrared spectra were recorded with an FT-IR 520 Nicolet Spectrophotometer. ^{1}H-NMR (δ(TMS) = 0.0 ppm), ^{31}P{^{1}H}-NMR (δ(85% H_3PO_4) = 0.0 ppm) spectra were obtained with a Varian Mercury 400, Bruker 400 and Bruker DMX 500. ES(+) mass spectra were recorded with a Fisons VG Quatro spectrometer. Absorption spectra were recorded with a Varian Cary 100 Bio UV-spectrophotometer and emission spectra with a Horiba-Jobin-Ybon SPEX Fluorolog 3.22 and Nanolog spectrofluorimeters. Microspectrofluorimetry measurements were carried out with a MicroSPEX instrument with the Spex Fluorog apparatus 3.22 connected to an Olympus BX51 M confocal microscope (Universidade Nova de Lisboa). Fluorescence microscopy was carried out with an Axioplan 2ie Zeiss imaging microscope equipped with a NikonDXM1200F digital camera (Universidade Nova de Lisboa) and a Leica DMIRB fluorescence microscope (Universitat de Barcelona). Optical microscopy was carried out with an Olympus BX51. Scanning electron microscopy was carried out at 5 kV using a Neon40 Crossbeam Station (Zeiss) equipped with a field emission gun. Cryo-transmission electron microscopy measurements were carreid out with a Tecnai G2 F20 (FEI) 200 kV FEG TEM cryomicroscope. A Horiba Scientific Nanoparticle Analyzer SZ-100 (Universidade Nova de Lisboa) operating at 25 °C was used to obtain the DLS measurements.

Preparation of the samples

Optical and fluorescence microscopy measurements. 1 mg of each compound was dissolved in 5 ml of each solvent. For the measurements, a drop of each solution was placed onto a microscope slide and evaporated to dryness.

SEM measurements. 4×10^{-4} M solutions of the complexes were used. A drop of each solution was deposited onto a silicon plate and evaporated to dryness by contact with air. This process was carried out in the same way for all of the different solvents.

Polarity effect studies. The solvents used were double-distilled water, methanol *p.a.* (Fluka), acetonitrile *p.a.* (Fluka), THF (appropriate drying agents), chloroform *p.a.* (Fluka), toluene (appropriate drying agents) and cyclohexane *p.a.* (Panreac).

To prepare solutions of **2**, **3**, and **5**, **6**, 1 mg of each compound was dissolved in 5 ml of each solvent, then the mother solutions were diluted to half concentration and the spectra were recorded. All of the measurements were made immediately after solution preparation as the coloring of these varies with time.

*Synthesis of [Au(acac)(PTA)] (**1a**).* Solid Tl(acac) (76 mg, 0.25 mmol) was added to a solution of [AuCl(PTA)] (100 mg, 0.25 mmol) in acetone (10 ml). After four days of stirring at room temperature, the resulting white suspension was filtered. The solution was concentrated to *ca.* 5 ml and *n*-hexane (10 ml) was added to precipitate [Au(acac)(PTA)] as a white solid which was filtered off and dried in vacuum. Yield: 71% (82 mg). ^{1}H-NMR (400 MHz, $CDCl_3$): 4.60–4.46 (AB q, J = 12 Hz, 6H, N–CH_2–N), 4.28 (s, 6H, N–CH_2–P), 2.25–2.12 (m, 8H, CH_3–(CO)–CH_2–(CO)–CH_3). ^{31}P{^{1}H}-NMR (162 MHz, $CDCl_3$): −45.1. IR (KBr, cm^{-1}): 1635 (C═O).

*Synthesis of [Au(acac)(DAPTA)] (**2a**).* Solid Tl(acac) (90 mg, 0.30 mmol) was added to a solution of [AuCl(DAPTA)] (120 mg, 0.30 mmol) in acetone (10 ml). After four days of stirring at room temperature, the white suspension was filtered. The resulting solution was concentrated to *ca.* 5 ml and *n*-hexane (10 ml) was added to precipitate [Au(acac)(DAPTA)] as a white solid which was filtered off and dried in vacuum. Yield: 73% (99 mg). ^{1}H-NMR (400 MHz, $CDCl_3$): 5.80 (d, J = 20.0 Hz, 1H, N–CH_2–N), 5.60 (dd, J = 20.0/12.0 Hz, 1H, N–CH_2–P), 4.96 (d, J = 16.0 Hz, 1H, N–CH_2–N), 4.80–4.60 (m, 2H, N–CH_2–P + N–CH_2–N), 4.15 (dt, J = 20.0/4.0, 1H, N–CH_2–P), 4.07 (d, J = 20.0 Hz, 1H, N–CH_2–N), 3.87 (s, 2H, N–CH_2–P), 3.57 (dt, J = 20.0/4.0 Hz, 1H, N–CH_2–P), 3.85 (s, 3H, N–CH_3), 1.85 (s, 6H, CO–CH_3), 2.25–2.12 (m, 8H, CH_3–(CO)–CH_2–(CO)–CH_3). ^{31}P{^{1}H}-NMR (162 MHz, $CDCl_3$): −48.3. IR (KBr, cm^{-1}): 1675 (C═O).

*Synthesis of [Au(C≡C-C_5H_4N)(CH_3PTA)]I (**1**).* CH_3I (0.12 ml, 0.19 mmol) was added dropwise to a solution of [Au(C≡C-C_5H_4N)(PTA)] (60 mg, 0.13 mmol) in CH_2Cl_2 (10 ml) at −40 °C. The suspension was allowed to warm to room temperature for 4 hours. The resulting pale yellow solution was concentrated to *ca.* 5 ml, and diethyl ether (10 ml) was added to precipitate a pale yellow solid. Yield: 80% (73 mg). ^{1}H-NMR (400 MHz, D_2O, ppm): 8.46 (d, J = 8.0 Hz, 2H, $H_{\alpha\text{-pyr}}$), 7.41 (d, J = 8.0 Hz, 2H, $H_{\beta\text{-pyr}}$), 5.08–4.90 (AB m, 4H, N–CH_2–N$^+$), 4.69–4.59 (AB m, 2H, N–CH_2–N), 4.56–4.44 (m, 2H, P–CH_2–N$^+$), 4.33–4.06 (AB, m, 4H, N–CH_2–P), 2.86 (s, 3H, N$^+$–CH_3). ^{31}P-NMR (162 MHz, D_2O, ppm): −57.2. IR (KBr, cm^{-1}): 3425 (C–H (CH_3)), 2100 (C≡C), 1664 (C═N). ES-MS (+) m/z: 471.10 ([M]+, calc.: 471.10). Elemental analyses for $C_{15}H_{23}AuIN_4P$ calc. %: C: 29.33, H, 3.77, N: 9.12; Found %: C: 29.42, H: 3.80, N: 9.31.

*Synthesis of [Au(C≡C-C_5H_4N-CH_3)(PTA)]I (**2**).* Solid [Au(acac)(PTA)] (40 mg, 0.08 mmol) was added to a solution of *N*-methyl-4-ethynylpyridine (10 mg, 0.08 mmol) in THF (10 ml). After 1 hour of stirring at room temperature, the resulting red solution was concentrated, and diethyl ether (10 ml) was added to precipitate a dark red solid. Yield: 75% (30 mg). ^{1}H-NMR (400 MHz, D_2O): 8.10 (d, J = 12.0 Hz, 2H, $H_{\alpha\text{-pyr}}$), 7.61 (d, J = 12.0 Hz, 2H, $H_{\beta\text{-pyr}}$), 4.67–4.50 (AB q, J = 16.0 Hz, 6H, N–CH_2–N), 4.37 (s, 6H, N–CH_2–P), 3.88 (s, 3H, CH_3). ^{31}P-NMR (162 MHz, $CDCl_3$, ppm): −48.2. IR (KBr, cm^{-1}): 3425 (C–H), 2104 (C≡C), 1640 (C═N). ESI-MS (+) m/z: 471.10 ([M]+, calc.: 471.10). Elemental analyses for $C_{15}H_{23}AuIN_4P$

calc. %: C: 29.33, H, 3.77, N: 9.12; Found %: C: 29.44, H: 3.81, N: 9.28.

*Synthesis of [Au(C≡C-C$_5$H$_4$N-CH$_3$)(DAPTA)]I (**3**).* Solid [Au(acac)(DAPTA)] (44 mg, 0.09 mmol) was added to a solution of *N*-methyl-4-ethynylpyridine (10 mg, 0.09 mmol) in THF (10 ml). After 1 hour of stirring at room temperature, the resulting red solution was concentrated, and diethyl ether (10 ml) was added to precipitate a dark red solid. Yield: 50% (23 mg). ^{1}H-NMR (400 MHz, D$_2$O): 8.80 (d, *J* = 12.0 Hz, 2H, H$_{\alpha\text{-pyr}}$), 7.70 (d, *J* = 12.0 Hz, 2H, H$_{\beta\text{-pyr}}$), 5.65 (d, *J* = 20.0 Hz, 1H, N–C*H*$_2$–N), 5.40 (dd, *J* = 20.0/12.0 Hz, 1H, N–C*H*$_2$–P), 5.10 (d, *J* = 16.0 Hz, 1H, N–C*H*$_2$–N), 4.70–3.88 (m, 7H, N–C*H*$_2$–P + N–C*H*$_2$–N + N–C*H*$_2$–P + N–C*H*$_2$–N + N–C*H*$_2$–P + N–C*H*$_2$–P), 3.76 (s, 3H, N–C*H*$_3$), 1.85 (s, 6H, CO–C*H*$_3$). ^{31}P{^{1}H}-NMR (162 MHz, CDCl$_3$, ppm): −17.2. IR (KBr, cm^{-1}): 3430 (C–H), 2100 (C≡C), 1937 (C═O), 1634 (C═N). ESI-MS (+) *m*/*z*: 543.12 ([M]+, calc.: 543.12). Elemental analyses for C$_{17}$H$_{23}$AuIN$_4$O$_2$P calc. %: C: 30.46, H, 3.46, N: 8.36; Found %: C: 30.49, H: 3.49, N: 8.41.

*Synthesis of [Au(C≡C-C$_5$H$_4$N)(CH$_3$PTA)](CF$_3$SO$_3$) (**4**).* CH$_3$CF$_3$SO$_3$ (4.1 μl, 0.36 mmol) was added dropwise to a solution of [Au(C≡C-C$_5$H$_4$N)(PTA)] (11 mg, 0.24 mmol) in CH$_2$Cl$_2$ (10 ml) at −40 °C. The suspension was allowed to warm to room temperature for 4 hours. The resulting pale yellow solution was concentrated to *ca*. 5 ml, and diethyl ether (10 ml) was added to precipitate a yellow solid. Yield: 80% (15 mg). ^{1}H-NMR (400 MHz, D$_2$O, ppm): 8.60 (d, *J* = 6.4 Hz, 2H, H$_{\alpha\text{-pyr}}$), 7.85 (d, *J* = 6.4 Hz, 2H, H$_{\beta\text{-pyr}}$), 5.10–4.92 (AB m, 4H, N–C*H*$_2$–N$^+$), 4.69–4.59 (AB m, 2H, N–C*H*$_2$–N), 4.54–4.45 (m, 2H, P–C*H*$_2$–N$^+$), 4.34–4.12 (AB, m, 4H, N–C*H*$_2$–P), 2.89 (s, 3H, N$^+$–CH$_3$). ^{31}P{^{1}H}-NMR (162 MHz, D$_2$O, ppm): −43.6. IR (KBr, cm^{-1}): 3433 (C–H (CH$_3$)), 2113 (C≡C), 1629 (C═N), 1264 (C–F). ES-MS (+) *m*/*z*: 471.10 ([M]+, calc.: 471.10). Elemental analyses for C$_{16}$H$_{23}$AuF$_3$N$_4$O$_3$PS calc. %: C: 30.43, H, 3.55, N: 7.89, S: 4.51; Found %: C: 3.59, H: 3.45, N: 7.80, S: 4.70.

*Synthesis of [Au(C≡C-C$_5$H$_4$N-CH$_3$)(PTA)](CF$_3$SO$_3$) (**5**).* Solid [Au(acac)(PTA)] (60 mg, 0.13 mmol) was added to a solution of *N*-methyl-4-ethynylpyridine triflate (43 mg, 0.15 mmol) in THF (10 ml). After 1 hour of stirring at room temperature the solution was concentrated to half volume and diethyl ether (10 ml) was added to precipitate a dark green solid. Yield: 68% (55 mg). ^{1}H NMR (CD$_3$OD, 400 MHz, ppm): 8.53 (d, *J* = 5.9 Hz, 2H, H$_{\alpha\text{-pyr}}$), 7.87 (d, *J* = 6.2 Hz, 2H, H$_{\beta\text{-pyr}}$), 4.71–3.85 (m, 15H, N–CH$_2$–N + N–CH$_2$–P + N–CH$_3$). ^{31}P{^{1}H}-NMR (162 MHz, CD$_3$OD, ppm): −27.0. IR (KBr, cm^{-1}): 2109 (C≡C), 1636 (C═N). ESI-MS(+) *m*/*z*: 471.10 ([M]$^+$ calc: 471.10). Elemental analyses for C$_{16}$H$_{23}$AuF$_3$N$_4$O$_3$PS calc. %: C: 30.20, H, 3.64, N: 7.89, S: 5.04; Found %: C: 30.52, H: 3.60, N: 7.81, S: 5.21.

*Synthesis of [Au(C≡C-C$_5$H$_4$N-CH$_3$)(DAPTA)](CF$_3$SO$_3$) (**6**).* Solid [Au(acac)(DAPTA)] (25 mg, 0.05 mmol) was added to a solution of *N*-methyl-4-ethynylpyridine triflate (15 mg, 0.05 mmol) in THF (5 ml). After 1 hour of stirring at room temperature the solution was concentrated to half volume and diethyl ether (10 ml) was added to precipitate a dark green solid. Yield: 70% (22 mg). ^{1}H NMR (CD$_3$OD, 400 MHz, ppm): 8.64 (d, *J* = 6.5 Hz, 2H, H$_{\alpha\text{-pyr}}$), 7.79 (d, *J* = 6.6 Hz, 2H, H$_{\beta\text{-pyr}}$), 5.71 (d, *J* = 13.9 Hz, 1H, N–CH$_2$–N), 5.54 (m, 1H, N–CH$_2$–P), 5.08 (d, *J* = 14.7 Hz, 1H, N–CH$_2$–N), 4.79–4.69 (m, 2H, N–CH$_2$–P + N–CH$_2$–N), 4.51–3.68 (m, 8H, N–CH$_2$–P (1H) + N–CH$_2$–N (1H), N–CH$_2$–P (2H) + N–CH$_2$–P (1H) + N–CH$_3$ (3H)), 2.10 (m, 6H, CO–CH$_3$). ^{31}P{^{1}H}-NMR (162 MHz, CD$_3$OD, ppm): −17.8. IR (KBr, cm^{-1}): 2116 (C≡C), 1635 (C═N). ESI-MS(+): *m*/*z*: 543.12 ([M]+, calc: 543.12). Elemental analyses for C$_{18}$H$_{23}$AuF$_3$N$_4$O$_5$PS calc. %: C: 31.22, H, 3.35, N: 8.09, S: 4.63; Found %: C: 30.97, H: 3.45, N: 7.95, S: 4.61.

Acknowledgements

The support and sponsorship provided by COST Action CM1005 is acknowledged. Authors are also grateful to the Ministerio de Ciencia e Innovación of Spain (Project ENE2015-63969-R). This work was also supported by the Associated Laboratory for Sustainable Chemistry-Clean Processes and Technologies-LAQV which is financed by national funds from FCT/MEC (UID/QUI/50006/2013) and co-financed by the ERDF under the PT2020 Partnership Agreement (POCI-01-0145-FEDER-007265). J. Ll. is a Serra Húnter Fellow and is grateful to the ICREA Academia program. This research was supported by a Marie Curie Intra-European Fellowship within the 7th European Community Framework Programme (R. G.).

References

1 S. Gupta and A. Saxena, *MRS Bull.*, 2014, **39**, 266.
2 D. Massiot, R. J. Messinger, S. Cadars, M. Deschamps, V. Montouillout, N. Pellerin, E. Veron, M. Allix, P. Florian and F. Fayon, *Acc. Chem. Res.*, 2013, **46**, 1975.
3 X. Zou, H. Ren and G. Zhu, *Chem. Commun.*, 2013, **49**, 3911.
4 A. G. Evans, J. W. Hutchinson, N. A. Fleck, M. F. Ashby and H. N. G. Wadley, *Prog. Mater. Sci.*, 2001, **46**, 309.
5 M. J. Mayoral Muñoz and G. Fernández, *Chem. Sci.*, 2012, **3**, 1395.
6 E. Y.-H. Hong, H.-L. Wong and V. W.-W. Yam, *Chem. Commun.*, 2014, **50**, 13272.
7 R. A. Bilbeisi, J.-C. Olsen, L. J. Charbonnière and A. Trabolsi, *Inorg. Chim. Acta*, 2014, **417**, 79.
8 Q.-F. Sun, J. Iwasa, D. Ogawa, Y. Ishido, S. Sato, T. Ozeki, Y. Sei, K. Yamaguchi and M. Fujita, *Science*, 2010, **328**, 1144.
9 C. P. Collier, E. W. Wong, M. Belohradsky, F. M. Raymo, J. F. Stoddart, P. J. Kuekes, R. S. Williams and J. R. Heath, *Science*, 1999, **285**, 391.
10 H. Schmidbaur and A. Schier, *Chem. Soc. Rev.*, 2012, **41**, 370.
11 J. C. Lima and L. Rodríguez, *Chem. Soc. Rev.*, 2011, **40**, 5442.
12 J. C. Lima and L. Rodríguez, *Inorganics*, 2015, **3**, 1.
13 A. Y.-Y. Tam and V. W.-W. Yam, *Chem. Soc. Rev.*, 2013, **42**, 1540.
14 P. Casuso, A. Pérez-San Vicente, H. Iribar, A. Gutiérrez-Rivera, A. Izeta, I. Loinaz, G. Cabañero, H.-J. Grande,

I. Odriozola and D. Dupin, *Chem. Commun.*, 2014, **50**, 15199.
15 R. Gavara, J. Llorca, J. C. Lima and L. Rodríguez, *Chem. Commun.*, 2013, **49**, 72.
16 E. Aguiló, R. Gavara, J. C. Lima, J. Llorca and L. Rodríguez, *J. Mater. Chem. C*, 2013, **1**, 5538.
17 A. J. Moro, B. Rome, E. Aguiló, J. Arcau, R. Puttreddy, K. Rissanen, J. C. Lima and L. Rodríguez, *Org. Biomol. Chem.*, 2015, **13**, 2026.
18 E. Y.-H. Hong, H.-L. Wong and V. W.-W. Yam, *Chem. – Eur. J.*, 2015, **21**, 5732.
19 C. Po, A. Y.-Y. Tam and V. W.-W. Yam, *Chem. Sci.*, 2014, **5**, 2688.
20 T. Fukino, H. Joo, Y. Hisada, M. Obana, H. Yamagishi, T. Hikina, M. Takata, N. Fujita and T. Aida, *Science*, 2014, **344**, 499.
21 F. García, P. A. Korevaar, A. Verlee, E. W. Meijer, A. R. A. Palmans and L. Sánchez, *Chem. Commun.*, 2013, **49**, 8674.
22 L. Rodríguez, C. Lodeiro, J. C. Lima and R. Crehuet, *Inorg. Chem.*, 2008, **47**, 4952.
23 J. Buendía and L. Sánchez, *Org. Lett.*, 2013, **15**, 5746.
24 T. Rudolph, N. K. Allampally, G. Fernández and F. H. Schacher, *Chem. – Eur. J.*, 2014, **20**, 13871.
25 X.-S. Xiao, W. Lu and C.-M. Che, *Chem. Sci.*, 2014, **5**, 2482.
26 H. Ito, T. Saito, N. Oshima, N. Kitamura, S. Ishizaka, Y. Hinatsu, M. Wakeshima, M. Kato, K. Tsuge and M. Sawamura, *J. Am. Chem. Soc.*, 2008, **130**, 10044.
27 V. J. Catalano, J. M. López de Luzuriaga, M. Monge, M. E. Olmos and D. Pascual, *Dalton Trans.*, 2014, **43**, 16486.
28 T. Lasanta, M. E. Olmos, A. Laguna, J. M. López de Luzuriaga and P. Naumov, *J. Am. Chem. Soc.*, 2011, **41**, 16358.
29 A. Laguna, T. Lasanta, J. M. López-de-Luzuriaga, M. Monge, P. Naumov and M. E. Olmos, *J. Am. Chem. Soc.*, 2010, **132**, 456.
30 D. B. Leznoff and J. Lefebvre, *Gold Bull.*, 2005, **38**, 47.
31 J. Vicente, M. T. Chicote and M. D. Abrisqueta, *Organometallics*, 1997, **16**, 5628.
32 E. Vergara, E. Cerrada, A. Casini, O. Zava, M. Laguna and P. J. Dyson, *Organometallics*, 2010, **29**, 2596.
33 R. Wanke, P. Smoleński, M. F. C. Guedes da Silva, L. M. D. R. S. Martins and A. J. L. Pombeiro, *Inorg. Chem.*, 2008, **47**, 10158.
34 E. Vergara, S. Miranda, F. Mohr, E. Cerrada, E. R. T. Tiekink, P. Romero, A. Mendía and M. Laguna, *Eur. J. Inorg. Chem.*, 2007, 2926.
35 A. Udvardy, A. Csaba Bényei and Á. Kathó, *J. Organomet. Chem.*, 2012, **717**, 116e122.
36 P. Smoleński, L. Benisvy, M. F. C. Guedes da Silva and A. J. L. Pombeiro, *Eur. J. Inorg. Chem.*, 2009, 1181.
37 L. M. D. R. S. Martins, E. C. B. A. Alegria, P. Smoleński, M. L. Kuznetsov and A. J. L. Pombeiro, *Inorg. Chem.*, 2013, **52**, 4534.
38 B. Kemper, Y. R. Hristova, S. Tacke, L. Stegemann, L. S. van Bezouwen, M. C. A. Stuart, J. Klingauf, C. A. Strassert and P. Besenius, *Chem. Commun.*, 2015, **51**, 5253.
39 T. H. T. Hsu, J. J. Naidu, B.-J. Yang, M.-Y. Jang and I. J. B. Lin, *Inorg. Chem.*, 2012, **51**, 98.
40 K. Holmberg, B. Jönsson, B. Kronberg and B. Lindman, *Surfactants and polymers in aqueous solution*, John Wiley & Sons, 2nd edn, 2002.
41 D. F. Evans and H. Wennerström, *The colloidal domain. Where physics, chemistry, biology and technology meet*, Wiley-VCH, New York, 1994.
42 L. Rodríguez, M. Ferrer, R. Crehuet, J. Anglada and J. C. Lima, *Inorg. Chem.*, 2012, **51**, 7636.
43 M. Ferrer, A. Gutiérrez, L. Rodríguez, O. Rossell, J. C. Lima, M. Font-Badía and X. Solans, *Eur. J. Inorg. Chem.*, 2008, **18**, 2899.
44 R. Gavara, E. Aguiló, C. Fonseca-Guerra, L. Rodríguez and J. C. Lima, *Inorg. Chem.*, 2015, **54**, 5195.
45 A. S. Abd-El-Aziz, C. E. Carraher, P. D. Harvey, C. U. Pittman and M. Zeldin, Macromolecules Containing Metal and Metal-Like Elements, in *Photophysics and Photochemistry of Metal-Containing Polymer*, John Wiley & Sons, 2010, vol. 10.
46 G. A. Heath and J. E. McGrady, *J. Chem. Soc., Dalton Trans.*, 1994, 3759.
47 C. Reichardt, *Solvents and Solvent Effects in Organic Chemistry*, Wiley-VCH, 470 Weinheim, 2003.
48 S. Bagheri and H. R. Masoodi, *Chem. Phys. Lett.*, 2015, **629**, 46.
49 S. K. Samanta and S. Bhattacharya, *J. Mater. Chem.*, 2012, **22**, 25277.
50 C. Y.-S. Chung and V. W.-W. Yam, *Chem. – Eur. J.*, 2014, **20**, 13016.
51 K. M.-C. Wong and V. W.-W. Yam, *Acc. Chem. Res.*, 2011, **44**, 424.
52 M. J. Kamlet and R. W. Taft, *J. Am. Chem. Soc.*, 1976, **98**, 377.
53 P. W. Carr, *J. Chromatogr.*, 1980, **194**, 105.
54 Y. Zhong, Z. Jiao and Y. Yu, *Biomed. Chromatogr.*, 2006, **20**, 319.
55 M. J. Kamlet, R. M. Doherty, R. W. Taft, M. H. Abraham and W. J. Koros, *J. Am. Chem. Soc.*, 1984, **106**, 1205.
56 L. Rodríguez, M. Ferrer, O. Rossell, F. J. S. Duarte, A. G. Santos and J. C. Lima, *J. Photochem. Photobiol., A*, 2009, **204**, 174.
57 N. Aliaga-Alcalde and L. Rodríguez, *Inorg. Chim. Acta*, 2012, **380**, 187.
58 A. L. Balch, *Gold Bull.*, 2004, **37**, 45.
59 M. A. Malwitz, S. H. Lim, R. L. White-Morris, D. M. Pham, M. M. Olmstead and A. L. Balch, *J. Am. Chem. Soc.*, 2012, **134**, 10885.
60 S. Kalgutkar and N. Castagnoli, *J. Med. Chem.*, 1992, **35**, 4165.
61 Z. Assefa, B. G. McBurnett, R. J. Staples, J. P. Fackler, B. Assmann, K. Angermaier and H. Schmidbaur, *Inorg. Chem.*, 1995, **34**, 75.
62 J. Vicente and M. Chicote, *Inorg. Synth.*, 1998, **32**, 172.
63 S. Rubinsztajn, W. K. Fife and M. Zeldin, *Tetrahedron Lett.*, 1992, **33**, 1821.

